Integrated triple gut hormone action broadens the therapeutic potential of endocrine biologics for metabolic diseases

Brian Finan[1–3*#], Bin Yang[3,4*], Nickki Ottaway[5], David L. Smiley[3], Tao Ma[3,6], Christoffer Clemmensen[1,2], Joe Chabenne[3,7], Lianshan Zhang[4], Kirk M. Habegger[8], Katrin Fischer[1,2], Jonathan E. Campbell[9], Darleen Sandoval[5], Randy J. Seeley[5], Konrad Bleicher[10], Sabine Uhles[10], William Riboulet[10], Jürgen Funk[10], Cornelia Hertel[10], Sara Belli[10], Elena Sebokova[10], Karin Conde-Knape[10], Anish Konkar[10], Daniel J. Drucker[9], Vasily Gelfanov[3], Paul T. Pfluger[1,2,5], Timo D. Müller[1,2], Diego Perez-Tilve[5], Richard D. DiMarchi[3#] & Matthias H. Tschöp[1,2,5#]

Nature Medicine: doi:10.1038/nm.3761

Supplemental Results

Chemical evolution from co-agonism to tri-agonism

The structural and sequence similarities amongst the three hormones (Fig. 1e), coupled with prior structure-function studies[1,2], informed the design of sequence hybridized peptides of high potency and balanced mixed agonism. The native hormones share nine conserved amino acids at positions 4, 5, 6, 8, 9, 11, 22, 25, and 26. These residues can be broadly grouped into two regions constituted by amino acids 4-11 and 22-26. The remaining central residues (amino acids 12-21) and the proximal terminal amino acids (1-3 and 27-30) exhibit more diversity that imparts the specificity of receptor interaction with each respective native hormone. Consequently, the challenge here is to maintain the individual affinity of each ligand for its receptor while eliminating the structural elements that convey selective preference for each individual receptor. Or stated differently, the objective here was the identification of a high affinity, promiscuous peptide for these three receptors.

Intermediary tri-agonist candidates were built from a glucagon-based core sequence with residues incorporated from GLP-1 that were previously shown to impart balanced and potent co-agonism at GLP-1R and GcgR[1]. This starting chimeric peptide features specific GLP-1 residues in the C-terminal portion at positions 17, 18, 20, 21, 23, and 24 (sequences of intermediate analogs displayed in Supplementary Figure 1 and mass spectrometry data is summarized in Supplementary Table 1). A series of peptide analogs was progressed in an iterative manner to introduce GIP agonism without destroying GLP-1R and GcgR potency. Each peptide was assessed for potency and maximal activity in a highly sensitive cell-based reporter gene assay that measured cAMP induction where one of the three human receptors was over-expressed in HEK293 cells (Table 1). In initial attempts to gain GIP activity, GIP-

specific N-terminal amino acids were individually and selectively introduced into peptide analogs of the parent, chimeric peptide. However, these GIP-derived substitutions, including Tyr^1 and Ile^7, which are well-characterized to be essential for native GIP activity[3], demonstrated little improvement in GIP potency (data not shown). Separately, Glu^3 substitution into the parent chimeric peptide, had noticeably enriched GIP character, but this resulted in a substantial reduction in potency at GcgR compared to the starting peptide (Table 1, peptide 9). Each of the three individual substitutions resulted in a concomitant loss of activity at the two other receptors, and in particular GcgR potency seemed most sensitive with the Glu^3 substitution being especially destructive, which is consistent with published reports[4,5]. This demonstrated that imparting sufficient GIP activity would not be trivial and suggested that extensive sequence modifications were essential to introduce the requisite triple agonism we desired. With the eventual intent of using these peptides for *in vivo* study, we considered the prospect of using site-specific lipidation to extend duration of biological action by promoting plasma albumin binding. As we have shown previously, site-specific lipidation can also serve as a chemical tool to enhance secondary structure and broaden biological activity[6]. We introduced a lysine at residue ten in the parent peptide to which a palmitic acid (C16:0), which was amidated through a single glutamic acid coupled at its gamma carboxylate (γE spacer). The suspected ability of the lipidation to stabilize secondary structure in a non-covalent manner that is analogous to what the lactam bond provides. One last change was the inversion of serine stereochemistry (d-Ser) at position two in order to render the analog resistant to dipeptidyl peptidase IV (DPP-IV)-mediated degradation, which is the endogenous enzyme responsible for N-terminal truncation of the first two amino acids of GLP-1, GIP, and glucagon. Secondly, this substitution at position two

also serves to preserve the potency at GcgR. This single peptide (Table 1, peptide 10) had a receptor activity profile similar to the starting peptide, but did not install any appreciable gain in GIPR agonism.

We had previously observed that enhanced alpha helical content is beneficial for inducing mixed agonism of GLP-1R and GcgR[1]. To determine if enhancing helicity likewise imparts GIPR agonism, further stabilization of the backbone helix within the aforementioned lipidated peptide (Table 1, peptide 10) was achieved with employment of an aminoisobutyric acid (Aib) substitution at position 16. Additionally and with the eventual intent for using these compounds *in vivo*, Aib was also employed at position two in order to convey resistance to DPP-IV inactivation in an analogous fashion as d-Ser. We have previously observed that Aib^2 also contributes to mixed agonism at GLP-1R and GIPR[2], however this substitution can be detrimental to glucagon activity. Therefore, a series of glucagon-specific residues were introduced to counter-act this anticipated loss in GcgR potency, which included Arg^{17}, Gln^{20}, and Asp^{28}, of which the latter substitution also enhances aqueous solubility in neutral pH buffers[7]. However, these cumulative substitutions (Table 1, peptide 11), despite preserving GcgR potency, did not introduce appreciable GIP activity when compared to the initial lipidated analog (Table 1, peptide 11).

In a parallel modification to the lipidated analog (Table 1, peptide 10), we included Aib^2, but we retained Glu^{16} instead of substitution with Aib^{16}. Glu^{16} likewise stabilizes the alpha helix through a non-covalent intra-helical interaction with Lys^{20} albeit to a lesser degree than Aib^{16}, as in **peptide 11**. Glu^{16} also provokes mixed agonism at GLP-1R and GcgR, and was thus retained to counterbalance the detrimental effects of Aib^2 on GcgR activity. We also included Leu^{27}, which is specific to native glucagon, in an additional attempt to boost glucagon activity. But

again much like the aforementioned previous attempts, these cumulative substitutions failed to enhance GIPR activity despite enhancing balanced, mixed agonism at GLP-1R and GcgR (Table 1, peptide 12). Each of these separate yet collective changes highlighted in **peptide 11** and **peptide 12** was investigated as a means to retain glucagon potency yet enhance GIP potency. Despite these failures in gaining GIP activity, these modifications led to the discovery of a high potency GLP-1/glucagon co-agonist with lipidation suitable for use *in vivo* and of enhanced solubility and chemical stability relative to the native hormones (Table 1, peptide 12). Nonetheless, the primary objective of balanced tri-agonism was no closer to a reality than when we started since **peptide 12** is reduced in GIP potency relative to the other two constituent activities by approximately one thousand-fold.

The structure-activity relationship (SAR) of position 2 was interrogated as we have previously reported the constructive interactions at this site with the central region of the peptide to change bioactivity[8]. To make a peptide backbone suitable for position 2 SAR without a subsequent loss of glucagon potency, a peptide scaffold was generated using several of the previously employed changes in the middle and C-terminal regions of **peptide 11** and **peptide 12**, including Glu^{16}, Arg^{17}, Gln^{20}, Leu^{27}, and Asp^{28}, all of which also serve auxiliary functions to enhance solubility and chemical stability. Additionally, in an attempt to selectively enhance GIP and glucagon activity, we introduced Asp^{21} and Val^{23}, which are each specific to native GIP and glucagon. Mixed agonism at GLP-1R and GcgR was preserved without an enrichment of agonism at GIPR (Table 1, peptide 13). Since the second amino acid influences selective activity at each constitutive receptor target, and also because the residues in the native sequences of GLP-1, GIP, and glucagon (alanine and serine) are both susceptible to *in vivo* proteolysis by DPP-IV[9,10], we chose amino acid

substitutions that retain a slightly different side chain composition, but one that was resistant to enzymatic cleavage. However, substitution with Aib^2, $dSer^2$, Gly^2, sarcosine (Sar^2), or $dAla^2$ did not appreciably change any of the constitutive receptor activity profiles (Table 1, peptides 13-17) such that unimolecular tri-agonism still remained elusive.

In discovering the dual GLP-1/GIP co-agonist, we observed that the terminal ends of the peptide need to be coordinately optimized to achieve high potency dual incretin receptor agonism[2]. Consequently, we inserted the three C-terminal residues of one of the endogenous forms of GLP-1, which included Gly^{29}, Arg^{30}, and Gly^{31}, into the $dSer^2$ containing **peptide 14** to generate an analog of 31-amino acid length (Table 1, peptide 18). These elongating substitutions impart a subtle gain in GIP activity that inspired further C-terminal extension of the peptide. Application of the C-terminal-extended (Cex) residues from exendin-4 to generate a 39-residue analog (Table 1, peptide 19) resulted in enhanced GIP activity and represents a breakthrough in the SAR to realize substantially higher GIP potency than the starting point peptide, or any of the aforementioned intermediate analogs. However, the GIP activity in **peptide 19** was unbalanced relative to its GLP-1 and glucagon counterparts, with an EC_{50} at GIPR that is of ~30-fold less relative potency (Table 1, peptide 19). Substitution with Aib^2 corrected this relative GIP imbalance to provide a unimolecular analog with a length identical to exendin-4, that is of exquisite potency and balance at each of the three receptors (Table 1, peptide 20). This peptide represents the first highly potent, balanced unimolecular triple agonist at GLP-1R, GIPR, and GcgR. Furthermore, this single molecule hybrid also possesses optimized chemical stability and pharmacokinetics due to site-specific acylation.

References

1 Day, J. W. *et al.* A new glucagon and GLP-1 co-agonist eliminates obesity in rodents. *Nature chemical biology* **5**, 749-757, doi:10.1038/nchembio.209 (2009).

2 Finan, B. *et al.* Unimolecular dual incretins maximize metabolic benefits in rodents, monkeys, and humans. *Science translational medicine* **5**, 209ra151, doi:10.1126/scitranslmed.3007218 (2013).

3 Moon, M. J. *et al.* Tyr1 and Ile7 of glucose-dependent insulinotropic polypeptide (GIP) confer differential ligand selectivity toward GIP and glucagon-like peptide-1 receptors. *Molecules and cells* **30**, 149-154, doi:10.1007/s10059-010-0100-5 (2010).

4 Runge, S., Wulff, B. S., Madsen, K., Brauner-Osborne, H. & Knudsen, L. B. Different domains of the glucagon and glucagon-like peptide-1 receptors provide the critical determinants of ligand selectivity. *British journal of pharmacology* **138**, 787-794, doi:10.1038/sj.bjp.0705120 (2003).

5 Pocai, A. *et al.* Glucagon-like peptide 1/glucagon receptor dual agonism reverses obesity in mice. *Diabetes* **58**, 2258-2266, doi:10.2337/db09-0278 (2009).

6 Ward, B., Ottaway N., Perez-Tilve D., Ma D., Gelfanov VM.,Tschop MH., and DiMarchi RD. Structural Changes Associated with Peptide Lipidation Broaden Biological Function. *Molecular metabolism*, doi:10.1016/j.molmet.2013.08.008 (2013).

7 Chabenne, J. R., DiMarchi, M. A., Gelfanov, V. M. & DiMarchi, R. D. Optimization of the native glucagon sequence for medicinal purposes. *Journal of diabetes science and technology* **4**, 1322-1331 (2010).

8 Patterson, J. T., Day, J. W., Gelfanov, V. M. & DiMarchi, R. D. Functional association of the N-terminal residues with the central region in glucagon-related peptides. *Journal of peptide science : an official publication of the European Peptide Society* **17**, 659-666, doi:10.1002/psc.1385 (2011).

9 Pospisilik, J. A. *et al.* Metabolism of glucagon by dipeptidyl peptidase IV (CD26). *Regulatory peptides* **96**, 133-141 (2001).

10 Kieffer, T. J., McIntosh, C. H. & Pederson, R. A. Degradation of glucose-dependent insulinotropic polypeptide and truncated glucagon-like peptide 1 in vitro and in vivo by dipeptidyl peptidase IV. *Endocrinology* **136**, 3585-3596 (1995).

Peptide #	Analog	GLP-1 Receptor			GIP Receptor			Glucagon Receptor		
		EC_{50} (nM)	STDev	Relative %	EC_{50} (nM)	STDev	Relative %	EC_{50} (nM)	STDev	Relative %
1	GLP-1	0.028	0.002	100	1513.825	78.950	0	2449.288	106.460	0
2	GLP-1 (Aib^2 E^{16} Cex K^{40}-C16 acyl) **"Acyl-GLP-1"**	0.015	0.001	187	122.883	10.668	0	162.402	29.771	0
3	GIP	1567.012	65.780	0	0.020	0.004	100	417.480	10.370	0
4	GIP (Aib^2 Cex K^{40}-C_{16} acyl) **"Acyl-GIP"**	6.330	2.690	0	0.012	0.001	168	2.920	0.840	1
5	Glucagon	3.100	0.494	1	1538.109	329.020	0	0.032	0.006	100
6	Glucagon (Aib^2 K^{10}-γEγE-C_{16} acyl Aib^{20}) **"Acyl-glucagon"**	0.479	0.068	6	22.650	6.100	0	0.005	0.001	625
7	**"GLP-1/GIP co-agonist"**	0.005	0.001	516	0.003	0.001	691	1.286	0.103	2
GIP SAR										
8	Glucagon (E^{16} Q^{17} A^{18} K^{20} E^{21} I^{23} A^{24})-NH_2	0.022	0.002	127	6.258	1.278	0	0.031	0.009	103
9	Peptide 8 (E^3)-NH_2	0.030	0.003	93	0.867	0.099	2	5.225	0.441	1
10	Peptide 8 (dS^2 K^{10}-γE-C16 acyl)-NH_2	0.039	0.005	72	2.691	0.416	1	0.041	0.002	78
11	Peptide 10 (Aib^2 Aib^{16} R^{17} Q^{20} D^{21} Q^{24} D^{28})-NH_2	0.015	0.003	187	2.194	0.329	1	0.028	0.009	114
12	Peptide 10 (Aib^2 E^{16} L^{27} D^{28})-NH_2	0.003	0.001	933	3.545	0.156	1	0.003	0.001	1067
Position 2 SAR										
13	Peptide 10 (Aib^2 R^{17} Q^{20} D^{21} V^{23} Q^{24} L^{27} D^{28})-NH_2	0.068	0.008	41	2.032	0.117	1	0.005	0.001	640
14	Peptide 13 (dS^2)-NH_2	0.003	0.001	933	1.654	0.164	1	0.006	0.001	533
15	Peptide 13 (G^2)-NH_2	0.093	0.013	30	1.103	0.200	2	0.005	0.001	640
16	Peptide 13 (Sar^2)-NH_2	0.115	0.014	24	5.828	0.334	0	0.016	0.003	200
17	Peptide 13 (dA^2)-NH_2	0.040	0.005	70	1.646	0.298	1	0.009	0.001	356
18	Peptide 14 (G^{29} R^{30} G^{31})-NH_2	0.002	0.001	1400	0.812	0.101	2	0.004	0.001	800
19	Peptide 14 (G^{29} Cex)-NH_2	0.002	0.001	1400	0.085	0.009	24	0.003	0.001	1067
20	Peptide 19 (Aib^2)-NH_2 **"Tri-agonist"**	0.003	0.001	933	0.003	0.001	673	0.004	0.001	800
Position 3 SAR										
21	Peptide 20 ($hSer^3$)-NH_2	0.003	0.001	933	0.004	0.001	505	0.016	0.002	200
22	Peptide 20 ($nVal^3$)-NH_2	0.003	0.001	933	0.002	0.001	1010	0.025	0.004	128
23	Peptide 20 (V^3)-NH_2	0.006	0.001	467	0.005	0.001	404	0.026	0.004	123
24	Peptide 20 ($nLeu^3$)-NH_2	0.003	0.001	933	0.003	0.001	673	0.033	0.003	97
25	Peptide 20 ($Dap(Ac)^3$)-NH_2	0.002	0.001	1400	0.010	0.002	202	0.043	0.006	74
26	Peptide 20 ($Met(O)^3$)-NH_2 **"Imbalanced tri-agonist"**	0.003	0.001	933	0.018	0.002	112	0.089	0.007	36
27	Peptide 20 (E^3)-NH_2 **"Matched co-agonist"**	0.004	0.001	700	0.002	0.001	1010	1.420	0.090	2
FLATT										
28	**YAG-Glucagon**	5.484	0.423*	1	1128.970	57.430*	0	3.270	0.109*	1
29	**[DA^2]GLP-1/GcG**	100.480	0.411*	0	17.110	0.920*	0	5.139	0.184*	1
RECIPROCAL										
30	**GLP-1/glucagon**	0.004	0.001	700	0.133	0.084	15	0.007	0.002	457
31	**GIP/glucagon**	0.568	0.192	5	0.004	0.001	505	0.008	0.003	400

Supplementary Table 1. *In vitro* human receptor activity profile of peptides. EC_{50} values represent the effective peptide concentrations (nM) that stimulate half-maximal activation at the human GLP-1, GIP, and glucagon receptors. STDev values represent the standard deviation of the calculated EC_{50} from each separate experiment. A minimum of three separate experiments was performed for each peptide at each respective receptor. Those peptides denoted with an asterisk (*) were only tested once at each respective receptor. Relative % activity at each receptor = (native ligand EC_{50}/analog EC_{50}) x 100. Continuing down from peptide 10, the peptides feature the same sequence of the peptide number denoted in the analog box with the subsequent modification contained within the parentheses. All sequences are found in Supplementary Figure 1.

Peptide #	Analog Name	Theoretical Mass	Observed Mass
1	GLP-1	3355.71	3357.1
2	GLP-1 (Aib^2 E^{16} Cex K^{40}-C16 acyl) **"Acyl-GLP-1"**	4429.06	4429.72
3	GIP	4855.46	4856.00
4	GIP (Aib^2 Cex K^{40}-C_{16} acyl) **"Acyl-GIP"**	4606.28	4606.37
5	Glucagon	3482.79	3483.40
6	Glucagon (Aib^2 K^{10}-γEγE-C_{16} acyl Aib^{20}) **"Acyl-glucagon"**	3868.42	3868.49
7	**"GLP-1/GIP co-agonist"**	4473.11	4473.14
GIP SAR			
8	Glucagon (E^{16} Q^{17} A^{18} K^{20} E^{21} I^{23} A^{24})-NH_2	3381.73	3382.19
9	Peptide 8 (E^3)-NH_2	3383.69	3384.10
10	Peptide 8 (dS^2 K^{10}-γE-C16 acyl)-NH_2	3714.25	3713.00
11	Peptide 10 (Aib^2 Aib^{16} R^{17} Q^{20} D^{21} Q^{24} D^{28})-NH_2	3726.27	3727.40
12	Peptide 10 (Aib^2 E^{16} L^{27} D^{28})-NH_2	3695.23	3694.50
Position 2 SAR			
13	Peptide 10 (Aib^2 R^{17} Q^{20} D^{21} V^{23} Q^{24} L^{27} D^{28})-NH_2	3727.25	3726.00
14	Peptide 13 (dS^2)-NH_2	3754.22	3753.00
15	Peptide 13 (G^2)-NH_2	3721.90	3720.50
16	Peptide 13 (Sar^2)-NH_2	3735.91	3735.00
17	Peptide 13 (dA^2)-NH_2	3738.22	3738.00
18	Peptide 14 (G^{29} R^{30} G^{31})-NH_2	3924.39	3924.16
19	Peptide 14 (G^{29} Cex)-NH_2	4546.03	4546.00
20	Peptide 19 (Aib^2)-NH_2 **"Tri-agonist"**	4543.08	4544.26
Position 3 SAR			
21	Peptide 20 ($hSer^3$)-NH_2	4516.05	4515.50
22	Peptide 20 ($nVal^3$)-NH_2	4528.11	4530.80
23	Peptide 20 (V^3)-NH_2	4528.11	4529.60
24	Peptide 20 ($nLeu^3$)-NH_2	4528.11	4528.00
25	Peptide 20 ($Dap(Ac)^3$)-NH_2	4543.08	4543.00
26	Peptide 20 ($Met(O)^3$)-NH_2 **"Imbalanced tri-agonist"**	4576.17	4577.47
27	Peptide 20 (E^3)-NH_2 **"Matched co-agonist"**	4544.06	4545.05
FLATT			
28	**YAG-Glucagon**	3259.54	3259.56
29	**[DA^2]GLP-1/GcG**	3556.01	3556.03
RECIPROCAL			
30	**GLP-1/glucagon**	3921.43	3922.39
31	**GIP/glucagon**	4484.18	4484.00

Supplementary Table 2. Mass profiles for peptide analogs. Theoretical and observed masses of each analog. Peptide molecular weights were determined electrospray ionization (ESI) or matrix-assisted laser desorption/ionization time-of-flight (MALDI-TOF) mass spectrometry, and character was confirmed by analytical reversed-phase high performance liquid chromatography (HPLC).

Species	Peptide	GLP1R		GIPR		GCGR	
		EC_{50} [nM]		EC_{50} [nM]		EC_{50} [nM]	
		Mean	SD	Mean	SD	Mean	SD
Mouse	**GLP-1/GIP co-agonist**	0.280	0.030	0.071	0.020	10.100	1.830
	Tri-agonist (peptide 20)	0.070	0.030	0.060	0.020	0.040	0.020
	Native Ligand	0.080	0.005	0.050	0.010	0.008	0.004
Rat	**GLP-1/GIP co-agonist**	0.124	0.080	0.040	0.016	20.317	11.390
	Tri-agonist (peptide 20)	0.060	0.030	0.030	0.010	0.090	0.030
	Native Ligand	0.050	0.005	0.010	0.007	0.032	0.016
Cyno	**GLP-1/GIP co-agonist**	0.117	0.070	0.109	0.105	28.585	2.425
	Tri-agonist (peptide 20)	0.060	0.010	0.080	0.030	0.090	0.020
	Native Ligand	0.080	0.040	0.030	0.010	0.190	0.030

Supplementary Table 3. cAMP production in CHO cells individually expressing recombinant mouse-, rat-, or cynomolgus monkey-derived GLP-1R, GIPR, or GcgR. EC_{50} values represent the effective peptide concentrations (nM) that stimulate half-maximal activation, as assessed by cAMP accumulation, at the mouse, rat, and cyno GLP-1, GIP, and glucagon receptors. SD values represent the standard deviation of the calculated EC_{50} from each separate experiment. A minimum of three separate experiments was performed for each peptide at each respective receptor from each species.

Receptor	Non-Specific Ligand	Radioligand	Cell Souce	Receptor Source	Incubation Time (min)	Incubation Temp (°C)	Specific Binding %	STDev	% Inhibition of Control
A1 Adenosine Receptor	DPCPX (1μM)	DPCPX (1nM)	CHO	Recombinant	60	RT	96.3	5.7	3.8
A2A Adenosine Receptor	NECA (10μM)	CGS (6nM)	HEK-293	Recombinant	120	RT	112.2	11.2	-12.2
A3 Adenosine Receptor	IB-MECA (1μM)	IB-MECA (0.15nM)	HEK-293	Recombinant	120	RT	127.2	7.7	-27.2
Alpha 1 Adrenergic Receptor	Prazosin (0.5μM)	Prazosin (0.25nM)	Rat Cortex	Endogenous	60	RT	105.7	2.5	-5.7
Alpha 2 Adrenergic Receptor	(-) Epinepherine (100μM)	RX 8211002 (0.5nM)	Rat Cortex	Endogenous	60	RT	109.1	28.6	-9.1
Beta 1 Adrenergic Receptor	Alprenolol (50μM)	CGP 12177 (0.3nM)	HEK-293	Recombinant	60	RT	92.6	8.4	7.5
Beta 2 Adrenergic Receptor	Alprenolol (50μM)	CGP 12177 (0.3nM)	CHO	Recombinant	120	RT	106.3	5.6	-6.3
Norepinepherine Transporter	Desipramine (1μM)	Nisoxetine (1nM)	CHO	Recombinant	120	4	111.5	6.3	-11.5
Angiotensin II Receptor Type 1	Angiotensin II (10μM)	Sar^1, Ile^4-Angiotensin II (0.05nM)	HEK-293	Recombinant	120	37	135.2	9.1	-35.2
Angiotensin II Receptor Type 2	Angiotensin II (10μM)	CGP 42112A (0.01nM)	HEK-293	Recombinant	240	37	101.0	5.2	-0.9
Central Benzodiazepine Receptor	Diazepam (3μM)	Flunitrazepam (0.4nM)	Rat Cortex	Endogenous	60	4	124.9	8.7	-24.9
Peripheral Benzodiazepine Receptor	PK 11195 (10μM)	PK 11195 (0.2nM)	Rat Heart	Endogenous	15	RT	108.1	7.7	-8.1
Bombesin Receptor	Bombesin (1μM)	Tyr^4-Bombesin (0.01nM)	Rat Cortex	Endogenous	60	RT	105.2	1.7	-5.2
Bradykinin Receptor B2	Bradykinin (1μM)	Bradykinin (0.3nM)	CHO	Recombinant	60	RT	101.6	3.9	-1.6
Calcitonin Receptor-Like Receptor	CGRPa (1μM)	CGRPa (0.03nM)	CHO	Recombinant	90	RT	112.5	9.3	-12.5
L-Type Calcium Channel	D 600 (10μM)	D 888 (3nM)	Rat Cortex	Endogenous	120	RT	117.8	0.7	-17.8
Small Conductance Calcium-Activated Potassium Channel	Apamin (100nM)	Apamin (0.007nM)	Rat Cortex	Endogenous	60	4	98.2	11.2	1.8
Cannabinoid Receptor Type 1	WIN 552312-2 (10μM)	CP559400.5nM)	CHO	Recombinant	120	37	111.4	6.4	-11.4
Cholecystokinin A Receptor	CCK (1μM)	CCK (0.08nM)	CHO	Recombinant	60	RT	111.9	4.8	-11.9
Cholecystokinin B Receptor	CCK (1μM)	CCK (0.08nM)	CHO	Recombinant	60	RT	120.4	9.3	-20.4
Dopamine Receptor D1	SCH 23390 (1μM)	SCH 23390 (0.3nM)	CHO	Recombinant	60	RT	111.2	0.4	-11.2
Dopamine Receptor D2	(+) Butaclamol (10μM)	Methyl-spiperone (0.3nM)	HEK-293	Recombinant	60	RT	94.0	3.1	6.0
Dopamine Receptor D3	(+) Butaclamol (10μM)	Methyl-spiperone (0.3nM)	CHO	Recombinant	60	RT	113.8	4.9	-13.8
Dopamine Receptor D4	(+) Butaclamol (10μM)	Methyl-spiperone (0.3nM)	CHO	Recombinant	60	RT	110.0	6.8	-10.0
Dopamine Receptor D5	SCH 23390 (10μM)	SCH 23390 (0.3nM)	GH4	Recombinant	60	RT	109.1	8.1	-9.1
Endothelin Receptor Type A	Endothelin-1 (100μM)	Endothelin-1 (0.03nM)	CHO	Recombinant	120	37	117.3	12.0	-17.3
Endothelin Receptor Type B	Endothelin-1 (0.1μM)	Endothelin-1 (0.03nM)	CHO	Recombinant	120	37	103.0	12.3	-3.0
Dopamine Transporter	BTCP (10μM)	BTCP (4.5nM)	CHO	Recombinant	120	4	103.1	0.6	-3.1
GABA Receptor	GABA (100μM)	GABA (10nM)	Rat Cortex	Endogenous	60	RT	103.5	6.6	-3.5
GABA-Gated Chloride Channel	Picrotoxinin (20μM)	TBPS (3nM)	Rat Cortex	Endogenous	120	RT	94.3	4.5	5.8
Galanin Receptor 1	Galanin (1μM)	Galanin (0.1nM)	HEK-293	Recombinant	60	RT	115.6	3.5	-15.6
Galanin Receptor 2	Galanin (1μM)	Galanin (0.05nM)	CHO	Recombinant	120	RT	99.8	1.8	0.2
Glucocorticoid Receptor	Triamcinolone (10μM)	Dexamethasone (1.5nM)	IM-9	Endogenous	360	4	100.5	3.1	-0.5
Glucagon Receptor	Glucagon (1μM)	Glucagon (0.025nM)	CHO	Recombinant	120	RT	23.3	5.9	76.7
Glucagon-Like Peptide 1 Receptor	GLP-1 (1μM)	GLP-1 (0.025nM)	BTC6	Endogenous	120	37	-5.6	4.7	105.6
Platelet-Derived Growth Factor Receptor	PDGF BB (10nM)	PDGF (0.3nM)	Balb/c 3T3	Endogenous	180	4	104.8	1.7	-4.8
Interleukin 8 Receptor	IL-8 (30nM)	IL-8 (0.025nM)	HEK-293	Recombinant	60	RT	101.3	0.0	-1.3
C-C Chemokine Receptor Type 1	MIP-1a (100nM)	MIP-1a (0.01nM)	HEK-293	Recombinant	120	RT	109.7	6.0	-9.7
Cluster of Differentiation 120	TNFa (10nM)	TNFa (0.1nM)	U-937	Endogenous	120	4	102.2	2.3	-2.2
Histamine H1 Receptor	Pyrilamine (1μM)	Pyrilamine (1nM))	HEK-293	Recombinant	60	RT	98.1	11.0	1.9
Histamine H2 Receptor	Tiotidine (100μM)	APT (0.075nM)	CHO	Recombinant	120	RT	120.4	7.1	-20.4
Melanocortin 4 Receptor	NDP-aMSH (1μM)	NDP-aMSH (0.05nM)	CHO	Recombinant	120	37	109.0	3.3	-8.9
Melatonin Receptor Type 1A	Melatonin (1μM)	2-Iodomelatonin (0.01nM)	CHO	Recombinant	60	RT	113.3	8.1	-13.3
Muscarinic Acetylcholine Receptor M1	Atropine (1μM)	Pirenzepine (2nM)	CHO	Recombinant	60	RT	133.1	5.0	-33.1
Muscarinic Acetylcholine Receptor M2	Atropine (1μM)	AF-DX 384 (2nM)	CHO	Recombinant	60	RT	110.1	6.2	-10.1
Muscarinic Acetylcholine Receptor M3	Atropine (1μM)	4-DAMP (0.2nM)	CHO	Recombinant	60	RT	103.2	3.8	-3.2
Muscarinic Acetylcholine Receptor M4	Atropine (1μM)	4-DAMP (0.2nM)	CHO	Recombinant	60	RT	117.7	13.1	-17.7
Muscarinic Acetylcholine Receptor M5	Atropine (1μM)	4-DAMP (0.3nM)	CHO	Recombinant	60	RT	108.7	8.2	-8.7
Tachykinin Receptor NK1	Sar^1, $Met(O^2)^{11}$-Substance P (1μM)	BH-Substance P (0.15nM)	U-373MG	Endogenous	60	RT	105.4	0.8	-5.4
Tachykinin Receptor NK2	$Nleu^{10}$-Neurokinin A (4-10) (300nM)	Neurokinin A (0.1nM)	CHO	Recombinant	60	RT	108.4	10.2	-8.4
Tachykinin Receptor NK3	SB 222200 (10μM)	SR 142801 (0.4nM)	CHO	Recombinant	120	RT	105.6	4.5	-5.6
Neuropeptide Y Receptor Y1	NPY (1μM)	Peptide YY (0.025nM)	SK-N-MC	Endogenous	120	37	103.6	1.1	-3.6
Neuropeptide Y Receptor Y2	NPY (1μM)	Peptide YY (0.015nM)	KAN-TS	Endogenous	60	37	113.3	7.1	-13.3
Neurotensin Receptor 1	Neurotensin (1μM)	Tyr^3-Neurotensin (0.05nM)	CHO	Recombinant	60	4	108.5	1.7	-8.5
N-Methyl-D-Aspartate Receptor	MK 801 (10μM)	TCP (10nM)	Rat Cortex	Endogenous	120	37	103.0	10.0	-3.0
Delta Opioid Receptor	Naltrexone (10μM)	DADLE (0.5nM)	CHO	Recombinant	120	RT	101.0	2.6	-0.9
Kappa Opioid Receptor	Naloxone (10μM)	U 69593 (1nM)	CHO	Recombinant	60	RT	109.2	8.1	-9.2
Mu Opioid Receptor	Naloxone (10μM)	DAMGO (0.5nM)	HEK-293	Recombinant	120	RT	100.4	5.0	-0.3
Nociceptin Receptor	Nociceptin (1μM)	Nociceptin (0.2nM)	HEK-293	Recombinant	60	RT	99.7	1.8	0.3
Pituitary Adenylate Cyclase-Activating Polypeptide Type 1 Receptor	PACAP (1-27) (100nM)	PACAP (1-27) (100nM)	CHO	Recombinant	120	RT	112.8	7.6	-12.8
Peroxisome Proliferator-Activated Receptor Gamma	Rosiglitazone (10μM)	Rosiglitazone (5nM)	E. coli	Recombinant	120	4	94.5	7.1	5.6
Voltage-Gated Potassium Channel	a-Dendrotoxin (50nM)	a-Dendrotoxin (0.01nM)	Rat Cortex	Endogenous	60	RT	112.2	1.0	-12.2
Prostaglandin E2 Receptor	PGE_2 (10μM)	PGE_2 (3nM)	HEK-293	Recombinant	120	RT	102.7	8.5	-2.7
Prostaglandin E4 Receptor	PGE2 (10μM)	PGE_2 (0.5nM)	HEK-293	Recombinant	120	RT	106.1	0.6	-6.1
Prostacyclin Receptor	Iloprost (10μM)	Iloprost (6nM)	HEK-293	Recombinant	60	RT	118.2	9.3	-18.2
Purinergic Receptor	dATPaS (10μM)	dATPaS (10nM)	Rat Cortex	Endogenous	60	RT	91.2	5.2	8.8
Purinergic Receptor P2X	a,B-MeATP (10μM)	a,B-MeATP (3nM)	Rat Bladder	Endogenous	120	4	101.6	0.9	-1.6
Serotonin Receptor HT_{1A}	8-OH-DPAT (10μM)	8-OH-DPAT (0.3nM)	HEK-293	Recombinant	60	RT	106.7	0.3	-6.7
Serotonin Receptor HT_{1B}	Serotonin (10μM)	CYP (0.1nM) / isoproterenol (30μM)	Rat Cortex	Endogenous	120	37	107.8	10.1	-7.7
Serotonin Receptor HT_{2A}	Ketanserin (1μM)	Ketanserin (0.5nM)	HEK-293	Recombinant	60	RT	104.5	4.7	-4.5
Serotonin Receptor HT_{2B}	(±) DOI (1μM)	(±) DOI (0.2nM)	CHO	Recombinant	60	RT	109.9	11.6	-9.9
Serotonin Receptor HT_{2C}	RS 102221 (10μM)	Mesulergine (1nM)	HEK-293	Recombinant	120	37	104.4	4.0	-4.3
Serotonin Receptor HT_3	MDL 72222 (10μM)	BRL 43694 (0.5nM)	CHO	Recombinant	120	RT	100.7	1.8	-0.7
Serotonin Receptor HT_{5A}	Serotonin (100μM)	LSD (1.5nM)	HEK-293	Recombinant	120	37	102.3	3.1	-2.3
Serotonin Receptor HT_6	Serotonin (100μM)	LSD (2nM)	CHO	Recombinant	120	37	103.3	4.0	-3.3
Serotonin Receptor HT_7	Serotonin (10μM)	LSD (4nM)	CHO	Recombinant	120	RT	118.4	7.4	-18.4
Serotonin Transporter	Imipramine (10μM)	Imipramine (2nM)	CHO	Recombinant	60	RT	109.1	6.6	-9.1
Sigma Receptor	Haloperidol (10μM)	DTG (10nM)	Jurkat	Endogenous	120	RT	105.4	1.6	-5.4
Somatostatin Receptor	Somatostatin (300nM)	Tyr^3-Somatostatin (0.05nM)	AtT-20	Endogenous	60	37	111.3	10.0	-11.3
Vasoactive Intestinal Polypeptide Receptor 1	VIP (1μM)	VIP (0.04nM)	CHO	Recombinant	60	RT	94.8	0.6	5.3
Arginine Vasopressin Receptor 1A	AVP (1μM)	AVP (0.3nM)	CHO	Recombinant	60	RT	95.1	2.8	5.0

Supplementary Table 4. *In vitro* receptor binding profile of the tri-agonist at off-target receptors. The GLP-1/GP/glucagon tri-agonist was screened for non-selective binding at 79 receptors or ion channels using customized high-throughput competitive binding assays. Results are expressed as % specific binding, calculated by [(tri-agonist specific binding / control specific binding) x 100], and also as % inhibition of control, calculated by [100 – (tri-agonist specific binding / control specific binding) x 100]. In general, results showing a % inhibition of control that is greater than 25% is considered a positive result of specific receptor binding and values less than 25% are considered a negative result of specific receptor binding. For each individual assay at the respective receptors, the ligand used to measure non-specific binding, the radioligand utilized to measure displacement from the receptor, the source of the receptor, and assay conditions are listed in the table. The tri-agonist was tested at a concentration of 1 μM and the non-specific ligands and radioligands were tested at the concentrations depicted in the table. A minimum of two separate experiments was performed for each respective receptor.

Nature Medicine: doi:10.1038/nm.3761

Cells	GLP-1	GIP	Glucagon	GLP-1/GIP Co-agonist	Tri-agonist (Peptide 20)
MIN6	0.45 ± 0.09	16.87 ± 4.00	31.29 ± 7.33	1.13 ± 0.56	0.81 ± 0.08
Rat hepatocytes	N/A	N/A	0.65 ± 0.55	21.32 ± 8.97	0.59 ± 0.29
3T3-L1 adipocytes	N/A	1.41 ± 0.30	N/A	0.53 ± 0.32	4.55 ± 5.61

Supplementary Table 5. Effects of the tri-agonist on cAMP production in cultured pancreatic β cells, hepatocytes, and adipocytes. Values represent mean EC_{50} ± standard deviation (nM) of cAMP production in the respective cell lines in response to a 30 min stimulation with the indicated peptides. Human GLP-1, GIP, and glucagon were used. A minimum of three separate experiments was performed for each peptide in each cell line.

Tri-agonist / peptide 20	Species				
	C57BL/6J Mice	DIO Mice	Rats	Dogs	Monkeys
Dose (mg/kg) / (nmol/kg)	0.045 / 10	0.045 / 10	0.045 / 10	ND	0.015 / 3
C_{max} (ng/ml)	195	636	34	ND	112
t_{max} (h)	4	2	2	ND	4
$t_{1/2}$ (h)	~5	~4	~6	ND	~5
GLP-1/GIP co-agonist	Species				
	C57BL/6J Mice	DIO Mice	Rats	Dogs	Monkeys
Dose (mg/kg) / (nmol/kg)	0.15 / 3	ND	1 / 222	0.045 / 10	0.045 / 10
C_{max} (ng/ml)	383	ND	480	90	55
t_{max} (h)	4	ND	4	4	6
$t_{1/2}$ (h)	~12	ND	~8	~6	~5

Supplementary Table 6. Pharmacokinetic comparison of the GLP-1/GIP co-agonist and the tri-agonist in different species. The pharmacokinetic parameters of the tri-agonist and the dual incretin co-agonist were determined following a subcutaneous injection of the peptides at the indicated doses in the different species. The concentration of the peptides in plasma was determined by LC-MS/MS and the pharmacokinetic analyses were determined by non-compartmental analysis with WinNonLin. C_{max}, maximal plasma concentration; t_{max}, time for maximal concentration, $t_{1/2}$, elimination half-life.

Supplementary Figure 1. Sequences of peptide analogs. Amino acid sequences of intermediate peptide analogs with the iterative residue substitutions from the preceding analog highlighted in blue. Aminoisobutyric acid is denoted as X. Lysine with a γE-C_{16} acyl attached through the side chain amine is denoted as underlined K. Sarcosine is denoted as #. D-enantiomers of select amino acids are italicized.

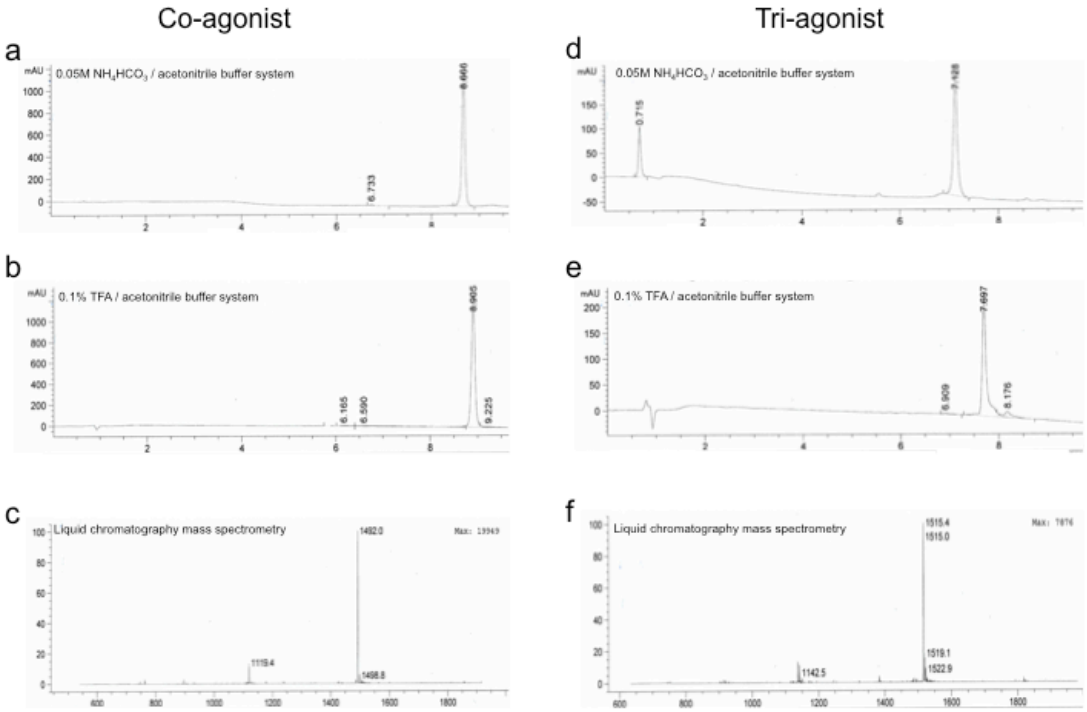

Supplementary Figure 2. HPLC and mass spectrometry. HPLC traces of the GLP-1/GIP co-agonist using a **(a)** basic buffer system and a **(b)** acidic buffer system. **(c)** LC-MS data of the GLP-1/GIP co-agonist. HPLC traces of the tri-agonist using a **(d)** basic buffer system and a **(e)** acidic buffer system. **(f)** LC-MS data of the tri-agonist.

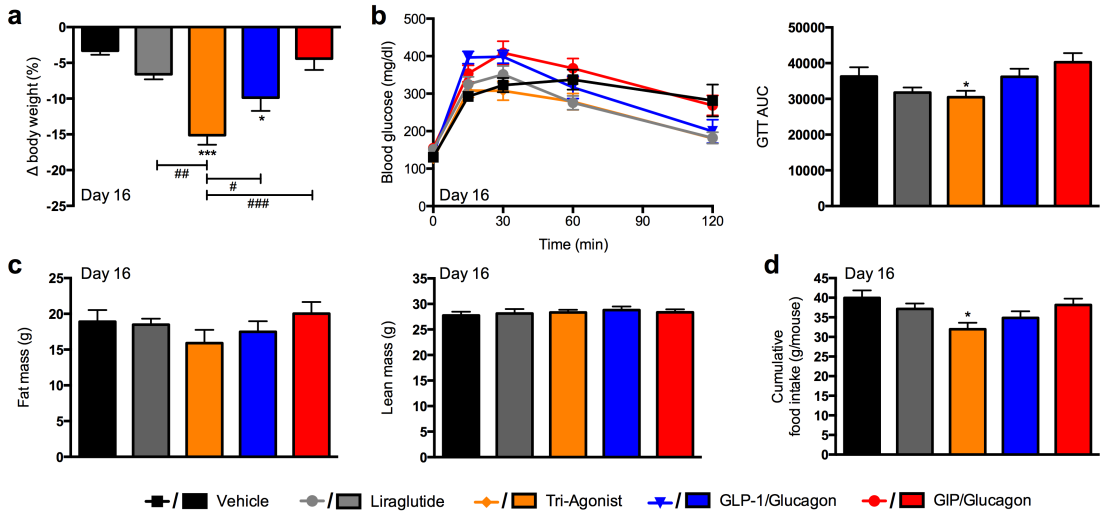

Supplementary Figure 3. Comparison to the tri-agonist to GLP-1/ glucagon and GIP/glucagon co-agonists. Effects on **(a)** body weight change, **(b)** glucose tolerance on day 16, **(c)** final body composition, and **(d)** cumulative food intake of male DIO mice treated with vehicle (black squares), liraglutide (gray circles), the GLP-1/GIP/glucagon tri-agonist (orange diamonds), a matched GLP-1/glucagon co-agonist (blue triangles), or a matched GIP/glucagon co-agonist (red circles). All mice were treated by daily subcutaneous injections at a dose of 3 nmoles kg^{-1}. Data in **(a–d)** represent means ± s.e.m. $^{*}P < 0.05$, $^{**}P < 0.01$, $^{***}P < 0.001$, determined by ANOVA comparing vehicle to compound injections, and $^{\#\#}P < 0.01$, $^{\#\#\#}P < 0.001$, determined ANOVA comparing tri-agonist injections to co-agonist injections. In both comparisons, ANOVA was followed by Tukey post hoc multiple comparison analysis to determine statistical significance.

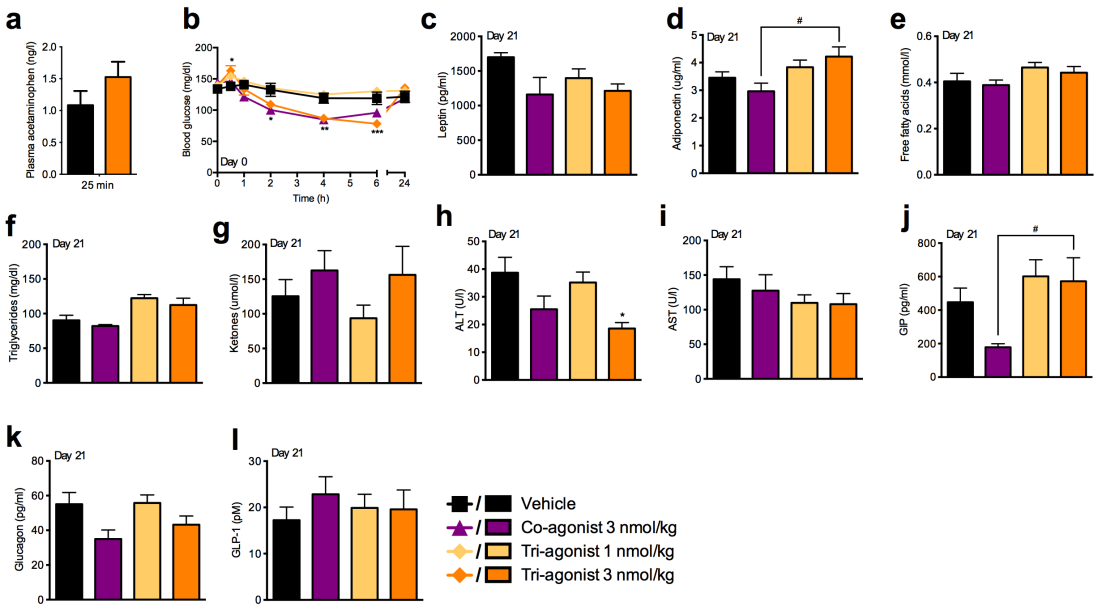

Supplementary Figure 4. Plasma analysis of DIO mice treated mice (complement to Figure 2). Effects on **(a)** plasma levels of acetaminophen 25 min. after oral gavage and 40 min. after injection of tri-agonist (3 nmoles per kg body weight). Effects on **(f)** blood glucose following a single bolus injection of compounds. Effects on plasma levels of **(c)** leptin **(d)** adiponectin, **(e)** free fatty acids, **(f)** triglycerides, **(g)** ketone bodies, **(h)** ALT, **(i)** AST, **(j)** total GIP, **(k)** glucagon, and **(l)** total GLP-1 of male DIO mice treated with vehicle (black), a dual incretin co-agonist (purple; 3 nmoles kg^{-1}), or a single molecular GLP-1/GIP/glucagon tri-agonist at 1 nmoles kg^{-1} (yellow) or 3 nmoles kg^{-1} (orange). All mice were treated by daily subcutaneous injections. Data in **(a–l)** represent means ± s.e.m. $^{*}P < 0.05$, determined by ANOVA comparing vehicle to compound injections, and $^{\#}P < 0.05$, determined ANOVA comparing dual incretin co-agonist to tri-agonist injections. In both comparisons, ANOVA was followed by Tukey post hoc multiple comparison analysis to determine statistical significance.

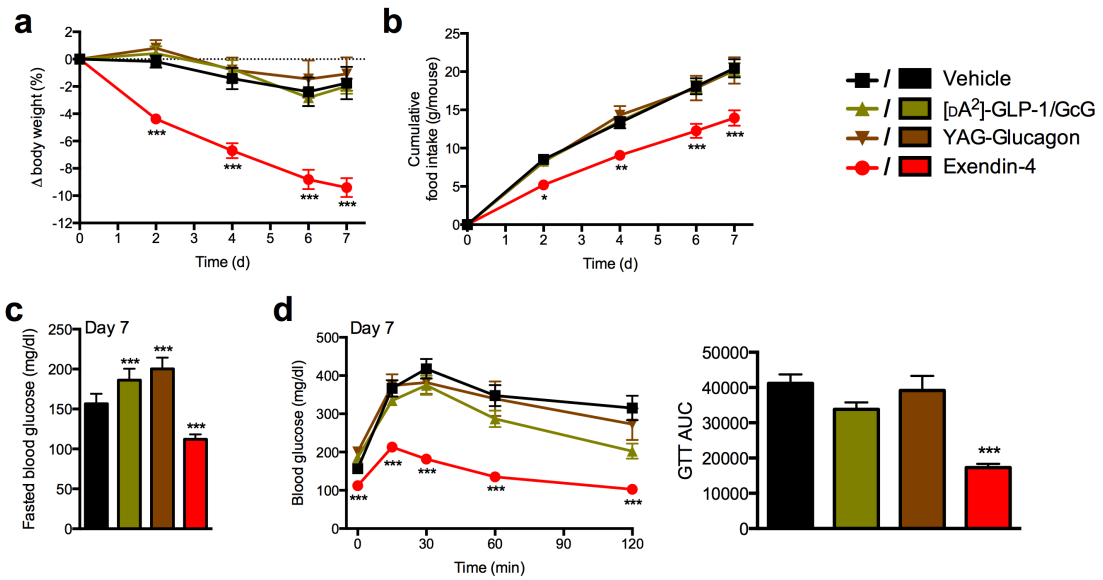

Supplementary Figure 5. Comparison to other purported triple agonists. Effects on **(a)** body weight change, **(b)** cumulative food intake, **(c)** fasted blood glucose, and **(d)** glucose tolerance of male DIO mice treated with vehicle (black squares), two different purported GLP-1/GIP/glucagon triple agonists: $_{D}A^{2}$-GLP-1/GcG (olive triangles) and YAG-glucagon (brown triangles), or exendin-4 (red circles). All mice were treated by twice daily subcutaneous injections (separated by 8 hours) at a cumulative dose of 50 nmoles kg^{-1} day^{-1} (2 x 25 nmoles kg^{-1}). Data in **(a–d)** represent means ± s.e.m. *$P < 0.05$, ** $P < 0.01$, *** $P < 0.001$, determined by ANOVA followed by Tukey post hoc multiple comparison analysis comparing vehicle to compound injections.

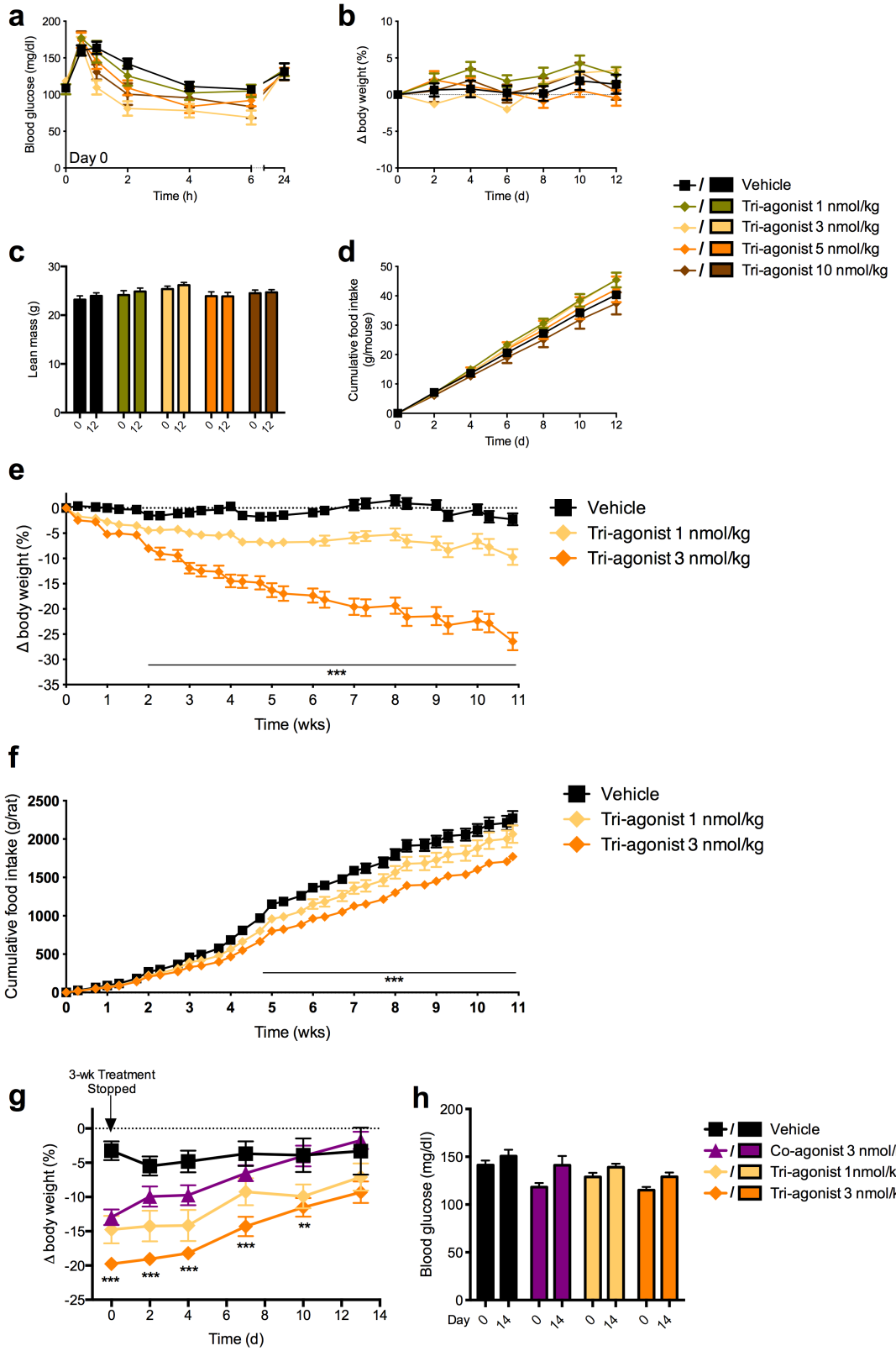

Supplementary Figure 6. Lack of acute hypoglycemia or long-term adverse effects with tri-agonist treatment. Effects on **(a)** acute fasted blood glucose, **(b)** body weight change, **(c)** lean mass, and **(d)** cumulative food intake of lean male C57Bl/6 DIO mice (n = 8 per group; age 6 months) treated with vehicle (black squares) or increasing daily doses of the tri-agonist at 1 (olive diamonds), 3 (yellow diamonds), 5 (orange diamonds), or 10 nmoles kg^{-1} (brown diamonds). Effects on **(e)**

body weight change and **(f)** cumulative food intake of DIO Long Evans rats treated 3-times per week with vehicle (black squares) or the tri-agonist at 1 or 3 nmoles kg^{-1} (yellow diamonds and orange diamonds, respectively). Effects on **(g)** body weight regain and **(h)** *ad libitum*-fed blood glucose of DIO male mice two weeks after treatment cessation. All mice were treated daily for 3 weeks with vehicle (black squares), a dual incretin co-agonist (purple triangles; 3 nmoles kg^{-1}), or a single molecular the tri-agonist at 1 nmoles kg^{-1} (yellow diamonds) or 3 nmoles kg^{-1} (orange diamonds). Data in **(a–h)** represent means ± s.e.m. *$P < 0.05$, ** $P < 0.01$, *** $P < 0.001$, determined by ANOVA followed by Tukey post hoc multiple comparison analysis comparing vehicle to tri-agonist injections.

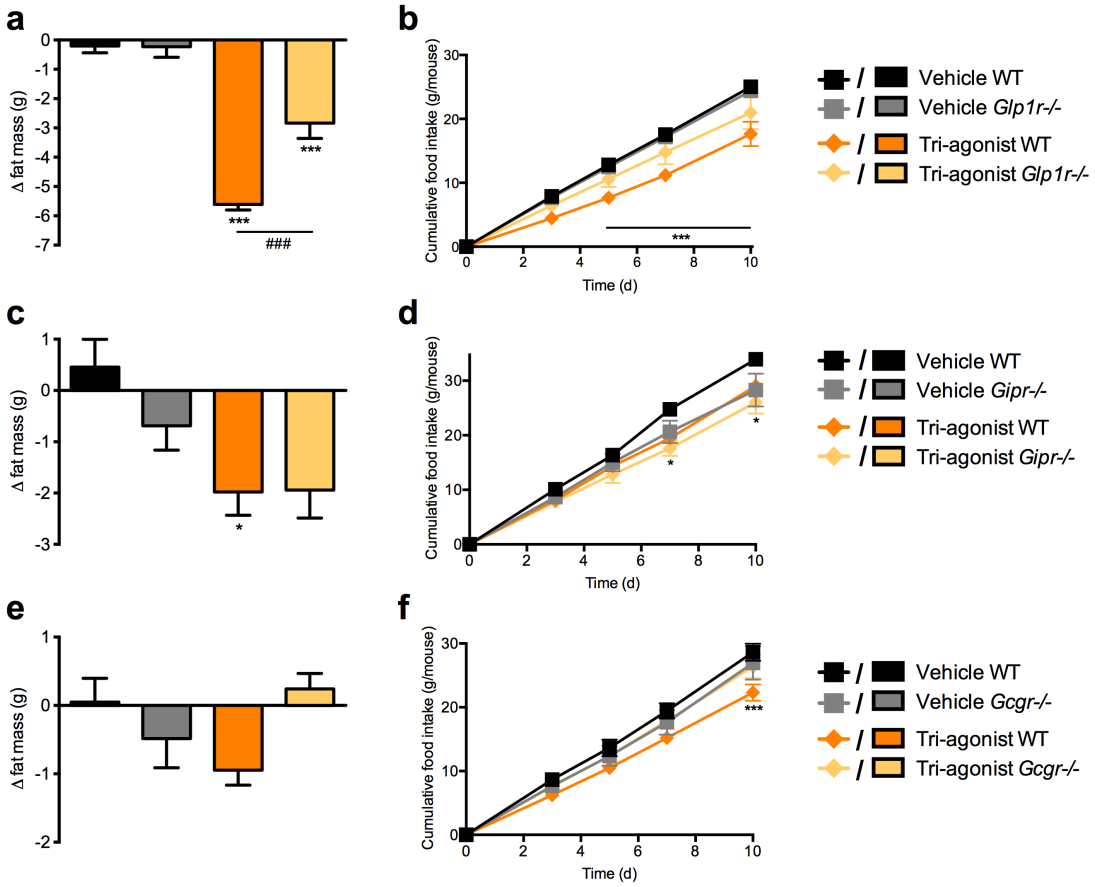

Supplementary Figure 7. The metabolic benefits of the tri-agonist are blunted in *Glp1r*–/–, *Gipr*–/–, and *Gcgr*–/– mice (complement to Figure 3). Effects on **(a)** fat mass change and **(b)** cumulative food intake in wild-type or *Glp1r*–/– male DIO mice. Effects on **(c)** body weight change and **(d)** cumulative food intake in wild-type or *Gipr*–/– male HFD mice. Effects on **(e)** body weight change and **(f)** cumulative food intake in wild-type or *Gcgr*–/– male HFD mice. All mice were treated every other day with vehicle (wt: black squares; ko: gray squares) or the tri-agonist (wt: orange diamonds; ko: yellow diamonds) at a dose of 10 nmoles kg^{-1}. Data in **(a–f)** represent means ± s.e.m. $^{*}P < 0.05$, $^{**}P < 0.01$, $^{***}P < 0.001$, determined by ANOVA comparing vehicle to compound injections within each genotype, and $^{\#}P < 0.05$, $^{\#\#}P < 0.01$, $^{\#\#\#}P < 0.001$, determined ANOVA comparing treatment of the tri-agonist between genotypes. In both comparisons, ANOVA was followed by Tukey post hoc multiple comparison analysis to determine statistical significance.

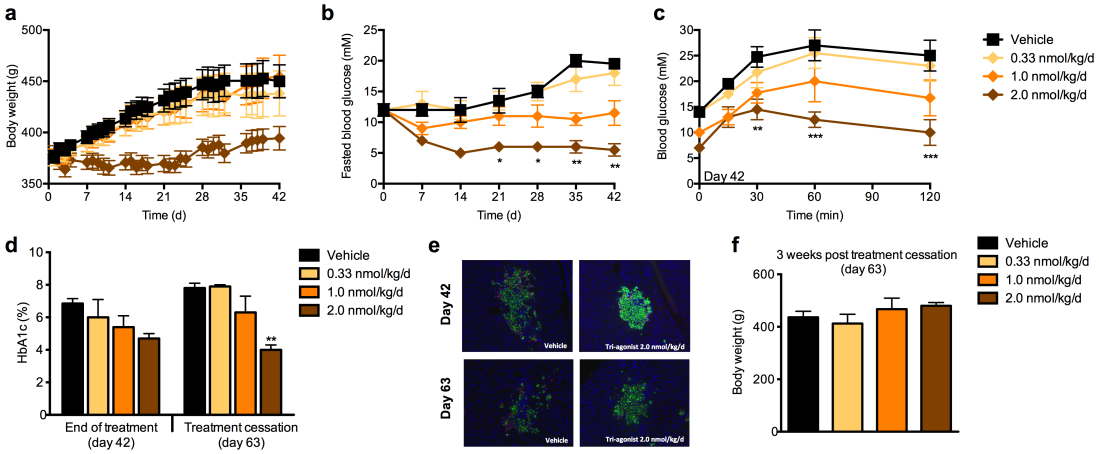

Supplementary Figure 8. Unimolecular GcgR, GLP-1R, and GIP triple agonism prevent hyperglycemia in ZDF rats. Effects on **(a)** body weight progression, **(b)** fasted blood glucose, **(c)** intraperitoneal glucose tolerance, **(d)** HbA1c, **(e)** islet cytoarchitecture and immunohistochemistry for insulin (green), glucagon (red), and Dapi staining (blue) following 6-weeks of treatment with escalating doses of the tri-agonist in male ZDF rats (age 9 weeks at start of study). Effects on **(d)** HbA1c, **(e)** islet cytoarchitecture and immunohistochemistry, and **(f)** body weight regain following 3 weeks of compound wash-out and 9 weeks after treatment initiation. Data in **(a–f)** represent means ± s.e.m. *$P < 0.05$, ** $P < 0.01$, *** $P < 0.001$, determined one- or two-way ANOVA followed by Tukey post hoc multiple comparison analysis to determine statistical significance comparing vehicle to tri-agonist injections.